Dynamic response of blast loaded Hollow Cylindrical and Truncated Conical Shells

N Mehreganian[1], Y Safa[2], G Boiger[2], E Nwankwo[3], AS Fallah[4,5]*

1. Department of Civil and Environment Engineering, University of Massachusetts Dartmouth, North Dartmouth, 02747 MA, USA

2. Institute of Computational Physics, School of Engineering, Zürich University of Applied Sciences, Technikumstrasse 9, 8400 Winterthur, Switzerland

3. Department of Civil Engineering, University of Benin, Benin city 300213, Edo State, Nigeria

4. Department of Machinery, Electronics and Chemistry, Oslo Metropolitan University, Pilestredet 35, 0166 Oslo, Norway

5. Department of Aeronautics, City and Guilds Building, South Kensington Campus, Imperial College London, UK

ABSTRACT

Hollow cylindrical and truncated conical shells depict enhanced torsional and shear resistance compared to beams and plates and are ubiquitously used in structures in aeronautics, submarines, wind turbines, pressure vessels, and transmission pylons. Upon extensive localised blast, these elements undergo local and global deformation and failure. The detrimental damage to the shell depends on the stand-off and charge mass and is proportional to the emerged local dynamic stresses and inelastic deformations. Large, localised translations relocate the structure's original pivot point and induce global rotations about the new one which raises the probability of structural collapse. In this work, we examine large plastic deformations of hollow cylindrical and truncated conical shells subject to a range of pulse pressures emanated from high explosives. Fluid-Structure Interaction (FSI)-based Finite Element (FE) models were developed to discern the characteristics of blasts at various stand-offs and functions were proposed to link load parameters to structural, material, and geometric properties.

1. INTRODUCTION

Hollow shells of initial curvature, such as cylindrical, hemispherical, and conical ones, have been extensively used as construction components of aerospace, chemical, nuclear, defense, mechanical, and civil engineering infrastructure, such as aircraft fuselages, wind turbine pylons, submarine hulls, tunnels, pressure vessels, transmission posts, etc. The shell's initial uniform curvature can provide additional torsional, bending, and shear resilience to resist accidental or intentional impact and pulse pressure loads. This is in particular a pronounced advantage when considering the concomitant reduction in weight as a result of hollowness. Recently, there has been a concerted effort to examine and mitigate the magnitude of localised blast or contact loads from proximal charges or high-velocity impacts, respectively, which due

*Corresponding Author: arashsol@oslomet.no

to the emerged concentrated stresses and large inelastic diametric deflections confined to the narrow zone on the interface, can induce catastrophic failure and damage to these structural elements.

Due to the wide applications of these shells in engineering, they may be subject to a variety of internal or external pulse pressure loads in different media: buried in soil, floating or submerged in water, or hovering or flying in air. The free-air and submerged blast analyses of the cylindrical shells have been performed extensively via experimentations or numerical FE analyses [1-9] investigating different aspects of this complex multiphysics phenomena. Closed-form analytical solutions have been developed by researchers (see e.g. [2], [10], [11]) for internal or external blasts using the constitutive framework of rigid-plasticity and Drucker-Prager bound theorems of limit analysis.

Confined internal blasts have been the subject of much research as they can intensify the impulse exerted on the target due to multiple reflections or cause pulsations in some cases. The pressure accumulation in the thin-walled rigid cylinders [12], pipelines [13], and tunnels [14] have also been examined experimentally for a wide range and varieties of explosive masses [15]. Thin-walled deformable cylinders have been experimentally examined since the early works of Duffey et al [16]. Langdon et. al [17], [18] observed longitudinal tearing in 330mm long stainless-steel cylindrical tubes of 150mm diameter, which were subjected to (partially) confined internal blasts generated from plastic explosive (PE4) charges at 60g and complete failure and pedalling with a 75g charge. These charges were positioned at the axial centre of the cylinders. The rupture impulse to induce the longitudinal tearing was calculated as 120N.s, which is 50% higher than the impulse threshold of square plates subjected to localised blasts.

Kwon and Fox [19] experimented on the unstiffened cylindrical shell subject to (distal) underwater blast and discussed three observed modes of deformation under such loading, namely, (i) the compression and subsequent release of the cylinder in the axial direction (referred to as 'accordion motion'), (ii) a 'whipping mode', wherein, following the indentation of the cylinder, it exhibits oscillatory motion which is governed by the curvature of the shock wave, and finally (iii) the residual (breathing) motion of the cylinder in the direction parallel to the shock wave. Brett [3] observed the characteristics of the underwater blasts as the spherical symmetry of bubble pulsation, time dependency of bubble diameter and reduction in bubble diameter. Yuen examined the multiphysics of the close-in air blast-loaded cylindrical shells both numerically and experimentally for different stand-offs. Both the indentation of the shell and imparted impulse reduced significantly with the increase of stand-off distance. For the blasts of identical stand-off, the increase of the explosive mass resulted in a larger indentation area and a higher central bulge in the cross-sectional profile of the shell.

Earliest studies on the conical shells date to Saunders in the 1960s [20] and Yang in 1974 [21] which examined the free and forced vibration of the shells. Liew et al. [10] examined the vibration of the doubly tapered cylindrical shell having a thickness reduction factor of α_y along the shell and found that the increase of α_y to unity (constant thickness) caused an initial decrease but subsequent increase in the natural frequencies of each mode, while the increase in the natural frequencies was monotonic. The increase in the shallowness parameter, i.e., the ratio of the rectangular planform width to the shell radius, simply increases the shell stiffness, hence increasing the natural frequencies. Sivadas and Ganesan [11] similarly examined the free vibration of the cylindrical shells with varying thickness but pointed out that the frequencies of the tapered circular cylindrical shells were greater than the corresponding frequencies of the cylindrical shell with constant thickness.

The dissemination of this paper is in 5 sections as follows: following this rather terse introduction, the dimensionless groups that govern the blast load properties are derived and discussed in Section §2. In §3 the methodology of the numerical FE analysis is presented, followed by presentation of the results and discussions in §4. Finally, in §5 the concluding remarks of the study are asserted and discussed.

2. DIMENSIONAL ANALYSIS

Dimensional analysis is a powerful tool to assess the physical characteristics of large-scale prototypes by relying on geometrically similar, smaller-scale models made of the same material and thus eliminating the need for experimentation on the prototypes. Furthermore, it significantly reduces the number of cases to be studied as many collapse on the same point in the dimensionless space. Such an analysis is developed for organising the experimental and numerical calculations to prevent repetitive results in the dimensionless numbers by using the Buckingham Π −theorem [21]. Ideally, when the external load acts on the homologous points of the two models, the use of scaling laws obviates the need to perform large-scale experimentation.

Jones and Li examined the sets of dimensional parameters which influence the dynamic response of rigid, perfectly plastic structural members subjected to impulsive loading [22], [23]. The authors stressed that as the transverse deflection of the structural member is expressed as a function of strain rate parameters, impulsive velocity and material characteristics, the material strain rate sensitivity cannot be merely described by Zhao's [24] response number $R_n = {I_e^2}/{\rho\sigma_0 h^2 \left(\frac{L}{h}\right)^2}$, in which I_e, ρ, and σ_0 are the Youngdahl's [25] mean impulse, mass density, and static yield stress, while L, h are the characteristic length and thickness of the structural member.

A series of dimensionless functions f_i, characterising the blast pressure on circular and quadrangular plates have also been derived by researchers [26], [27]. Nurick and co-author [28]–[35] have performed several experimental and numerical analyses on the influences of explosive shape, V-shaped plate angle, and stand-off distance on the localised and global blast loads. The linear relationship between the dimensionless permanent transverse displacement of the plate and the dimensionless impulse ϕ establishes a baseline approach to predict the structural response in the localised blast loads.

It should, however, be noted that while the shape of the explosive would affect the total impulse imparted on the target, the condition where the geometrical configuration affects the imparted impulse is pertinent to the non-prismatic manifolds [33] such as Inverted Truncated Cone (ITC) explosives. As the cylindrical explosives induce blast pressures which propagate ideally in direction of their central axis, the variation in charge height has a significant effect on the imparted impulse. However, the response of the target from the detonation of different charge shapes is beyond the scope of this study.

In this work, it is assumed that the blast pressure is induced by a PE4 cuboid explosive of mass M_e, with the specific heat of the explosion $Q_e = 8135 J/kg$ [36], at a stand-off S_d, half-length L_e, and half-width of $B_e = L_e$. The height of the explosive h_e is dependent on its side length as $h_e = M_e/4\rho_e L_e^2$, where ρ_e is the explosive density. Thus, the four independent

parameters which can fully describe the blast source are Q_e, S_d, L_e, M_e. Provided the cuboid explosive exerts the same impulse as a disk explosive of equivalent diameter $D_{eq} = 4L_e/\sqrt{\pi}$ and same charge height, the dimensionless function delineating the blast pressure amplitude P_0 is then determined by using the Buckingham Π-theorem [27], [37], (with Young's modulus E and the speed of sound through solid as $a_0 = \sqrt{E/\rho}$), as:

$$\Pi_1 = \frac{P_0 a_0^{-2} D_e}{M_e}, \tag{1}$$

which can be rewritten as:

$$P_0 = M_e a_0^2 f_1\left(\frac{S_d}{D_e}\right), \tag{2}$$

where $D_e = 2L_e$ herein, while f_1 is a dimensionless function which can be evaluated through curve-fitting tools applied to experimental or numerical data.

The pulse pressure load can be idealised to be expressed as a multiplicative decomposition of its spatial part (load shape) and the temporal part (pulse shape), truncated into its first term as $p(l, z, t) = P(l, z)p_3(t)$, over the cylindrical coordinates r, θ, z, with $l = R\theta$ being the arc length across the shell surface and R the shell's characteristic radius. Concerning the pulse shape (temporal part), various profiles may be assumed (linear, rectangular, sinusoidal, exponential), although the exponential pulse shape is more consistent with blast pressures of high explosives, which is given as:

$$p_3(t) = \exp(-Xt) \tag{3}$$

The total impulse imparted to the structure, corresponding to the positive phase of the blast pressure, and ignoring the effect of the negative phase is expressed as:

$$I_s = \int_0^{t_d} \int_A P(l, z)p_3(t)dAdt \tag{4}$$

Over the elemental area A ($dA = Rd\theta dl$), and with $P(l, z) = P_0 p_1(l)p_2(z)$, while z denotes the generalised coordinate in the direction of the shell's axis of symmetry.

For the cylindrical shells, provided the pressure variation along the generalised coordinate z assumes the same load shape (see Figure 2) for every generalised coordinate θ, i.e., the decay profile of the load across z from every peripheral material mesh point on the surface S to be the same, Eq. (4) can be recast into:

$$I_s = 2R \int_0^{t_d} \int_0^{\pi} \int_0^{L} P_0 p_1(\theta)p_2(z)p_3(t)dzd\theta dt = P_0 i_t i_\theta i_z, \tag{5}$$

where i_t, i_θ, i_z are functionals of the pulse shape and load shape profile functions over the temporal and spatial coordinates t, θ, z, respectively. Provided the target is discretised with a either non-uniform (Eq. (6)) or uniform (Eq. (7)) mesh, the discrete form of Eq. (5) becomes:

$$I_s = 2RP_0 i_t \sum_{k=1}^{n}\sum_{q=1}^{m} p_1(\theta_k) p_2(z_q)\, \Delta\theta_k \Delta z_q, \tag{6}$$

$$I_s = A_{el} P_0 i_t \sum_{k=1}^{n}\sum_{q=1}^{m} p_1(\theta_k) p_2(z_q), \tag{7}$$

Eq. (6) is valid for cylindrical and conical shells but could be simplified to Eq. (7) for a cylindrical shell, where A_{el} is the elemental area. To calculate the impulse I_s from Eq.(5), the pressure time histories registered with the gauge points of the shell were captured. This will render possible the calculation of the integral form (Eq. (5)) if approximating functions are used or the discrete form (Eqs. (6,7)) if the data registered are directly used.

Jones [23], [38] defined dimensionless kinetic energy for plates as:

$$\Pi_2 = \lambda = \frac{\mu V_0^2 L^2}{\sigma_0 h^3} = \phi^2, \tag{8}$$

where V_0 is the impulsive velocity, σ_0 the static plastic collapse stress, $\mu = \rho h$ the mass areal density of the plate (mass per unit area), L the half-length of the square plate and ϕ the dimensionless impulse. For the blasts that are impulsive, the term $\mu V_0 = P_0 t_d$, with t_d representing the duration of the pulse for the impulse I_s imparted on the target structure. For the conical and cylindrical shells, the term L^2 may be replaced with the surface area of the shell A_s. To account for the influence of the charge radius, Nurick and Martin [31] developed a dimensionless impulse parameter $\phi_c = \phi\gamma$, with $\gamma = 1 + \ln\left(4L^2/\pi D_e^2\right)$, with D_e being the diameter of the explosive disk. For the shells studied here we incorporate the charge radius and plate characteristic length, which may be modified and used for the shells as:

$$\begin{aligned} \phi_c &= \frac{I_s \gamma}{H^2\sqrt{A_S \sigma_0 \rho}}, \\ \gamma &= 1 + \ln(A_s \,/\, A_e\,), \end{aligned} \tag{9}$$

where $A_e = \pi D_e^2/4$ is the explosive area. Eq. (8) may be further amended to account for the influence of stand-off as proposed by Jacob et al [35] as:

$$\begin{aligned} \phi_{sd} &= \phi_c \gamma_{Sd}, \\ \gamma_{sd} &= 1 + \ln\left(\frac{2S_d}{D_e}\right) \end{aligned} \tag{10}$$

While similar dimensionless functions are possible by replacing the characteristic parameters of f_1 (and similar expressions) with those of identical dimensions(h_e, L instead of D_e), it is straightforward to show that the functions of interest $f_1,\ i_t, I_s$, as well as $\overline{W} = W/h$ herein, can be expressed as dimensionless functions of stand-off distance to charge diameter ratio (s_d/D_e), giving $\phi_{sd} = f_2\left(\frac{S_d}{D_e}, \overline{W}\right)$ and $i_t = f_3\left(\frac{S_d}{D_e}\right)$. The parameter $\overline{W} = W/h$ represents the maximum dimensionless deformation of the shells, with W the maximum

diametric deflection of the shell at the tip of the contact interface. The analysis results may thus be implemented in the built-in curve-fitting tools of MATLAB or similar software to quantify the parameters of these functions.

3. NUMERICAL SIMULATIONS USING FE MODELS INCLUDING FSI

Full 3-Dimensional Finite Element (FE) models were developed in ABAQUS Explicit commercial hydrocode to assess the transient deformation of the blast-loaded cylindrical and TC shells governed by Fluid-Structure Interaction (FSI). To this end, similar to the work of [39]–[41] we rely on the Multi-Material-Arbitrary Lagrangian-Eulerian technique, in which the Eulerian processor and Lagrangian processor work side by side to handle complex FSI problems. The Eulerian manifold, which is typically fixed in space, encompasses the multi-materials, i.e., the explosive, the medium (air) and the target shell. The former two materials occupy an equivalent fraction of the Eulerian medium mesh and are thus handled by the Eulerian processor, while the target shells can be handled with the Lagrangian processor.

Upon detonation of the explosive, the solid constituent particles instantaneously turn into gaseous products, whereby the generated pressure wave propagates through the Eulerian fluid (air) particles. At the instant of contact with the Lagrangian elements, the FSI algorithms (continuity at the interface) are invoked which cause the transmission of the pressure to the target. This technique, commonly known as Coupled Eulerian-Lagrangian (CEL), can provide relatively accurate information on the transient deformation of the flexible structure in accordance with the experimentations, although the measurements of the pressure time histories using this method are intrinsically difficult, if not impossible. On the other hand, the state variable (pressure) values can be captured by consideration of the rigid target in place of the flexible one, by prescribing rigid boundary conditions (BC) to the gauge points of the Eulerian medium where the flexible Lagrangian structure would have lain. This method is referred to as the Uncoupled Eulerian-Lagrangian as the pressure registered with the gauge points can also be implemented to the corresponding elements of the flexible structure in a separate model. It should however be noted that, due to the FSI effects, the calculated impulse and pressure of UEL would lead to an overestimation of the actual response from the Coupled method [17], [42]–[44]. In this work, the UEL models were performed on the cylindrical and truncated conical shells.

Table 1. Material properties for the FSI models (from [27], [45])

PE-4 $\boldsymbol{\rho_e}$ **=1601**	**JWL EOS (values from Ref. [17], [40]**						
	v (ms^{-1})	A (GPa)	B (GPa)	R_1	R_2	ω	E_m (Mj)
	8193	60.977	12.95	4.5	1.4	0.25	6.057
Air $\boldsymbol{\rho_a}$ **=1.293**	**Ideal Gas Law EOS**						
	ν_k(μ. Pa. s)	C_v(J/kgK)	R'(J/kg. K)	P_a (Pa)			
	18.27	717.6	287	101325			
Steel materials	**Johnson Cook failure parameters**						
		A_1(MPa)	B_1(MPa)	C	n		m
Mild steel, $\boldsymbol{\rho = 7850}$		325	275	0.076	0.36		1

For the cylindrical shells, to reduce the computation time, an axisymmetric cuboid of 150×300×400mm was created for the Eulerian medium, as shown in Figure , and was discretised with a hexahedral E3D8R mesh of 4mm element length. The transmission boundaries of the Eulerian manifold were associated with the free outflow condition, while the inflow condition was prescribed to the lowest side of the Eulerian cuboid. For the UEL model of cylindrical shells, the positions of the explosive and shell were swapped, and rigid BCs were prescribed to the lowest face of the Eulerian cube. Concerning the geometrical configuration of the CEL and UEL models for the TC shells, the Eulerian medium had a smaller size of 200×200×400mm but was discretised with the same element type and size as for the cylindrical models. Such extended configuration was chosen to encompass the shell- the tip of which was permitted to displace freely- and the full-sized explosive, but rather with free outflow instead axisymmetric boundary conditions on the front face. In the UEL model of the TC shell, the gauge points were positioned at the upper face with rigid boundary conditions (Figure (b)). Concerning the Equation Of State (EOS) of the multi-materials, the air was modelled as an ideal gas, described by the ideal gas model $P_a = (C_P - C_v)\rho_a T$, with C_p, C_v ρ_a and T being the specific heat at constant pressure and volume, air density, and temperature, respectively, while R' and P_a in Table 1 represent the ideal gas constant ambient pressure for air. The explosive material, on the other hand, was described by the Jones-Wilkins-Lee (JWL) EOS [17], whose parameters are summarised in Table 1. The reader is referred to [17] for further discussion on the EOS of the air and the explosive.

The explosive used was a cube of PE4 with a half-length/width of $L_e = B_e$ =25mm and the constant charge height of 12.5mm, giving the charge a total mass of 50.013g. The explosive was assumed to detonate instantaneously and from its mass centre (zero time for the shock wave to travel from the centroid to the boundaries). The stand-off distance, measured from the top fibre of the explosive to the closest target point on the shell, varied between 37.5mm and 187.5mm in increments of 25mm. The choice of stand-off ensures a range of blast loads from localised to global and supplements the authors' previous works [27], [46]. For these blast scenarios, the Hopkinson Cranz scale distances ($Z[m/kg^{\frac{1}{3}}]$), assuming a TNT equivalence coefficient of 1.31 for PE4 (inducing the same overpressure), is calculated as Z =0.093, 0.217, 0.314 and 0.293, in an ascending order of the stand-off distance.

The target cylinders were 180mm long and had a radius of 100mm. A 30mm length of the cylinder which extended out of the Eulerian cube was clamped to two fixed rigid cylinders. The TC shells had a base of $R_1 = 40mm$ which linearly reduced to $R_2 = 20mm$ at the height of $h_1 - h_2 = 150mm$ (Figure e). The surface area of the truncated cone was thus given as:

$$A_s = \frac{3}{4}\pi R_1 \sqrt{R_1^2 + h_1^2} \tag{11}$$

Similar to the cylindrical shell counterparts, the end face of the TC shells was extended by 30mm to allow a tied connection to the clamps of the same height (see Figure 1).

The shells were made of mild steel and were prescribed by Johnson Cook constitutive plasticity model in which the dynamic yield σ_0 is cast into a multiplicative decomposition of functions of the strain, strain rate, and temperature, given explicitly as

$\sigma_0 = (A_1 + B\varepsilon^n)(1 + Cln\dot{\varepsilon}^*)(1 + T^{*m})$. The parameters A_1, B and n are the first static plastic yield, plastic flow stress constant and exponent, respectively, while C represents the strain rate sensitivity coefficient, and $\dot{\varepsilon}^*$ is the quotient of the dynamic plastic strain rate to the reference plastic strain rate, while T^* and m are the homologous temperature and its exponent, respectively.

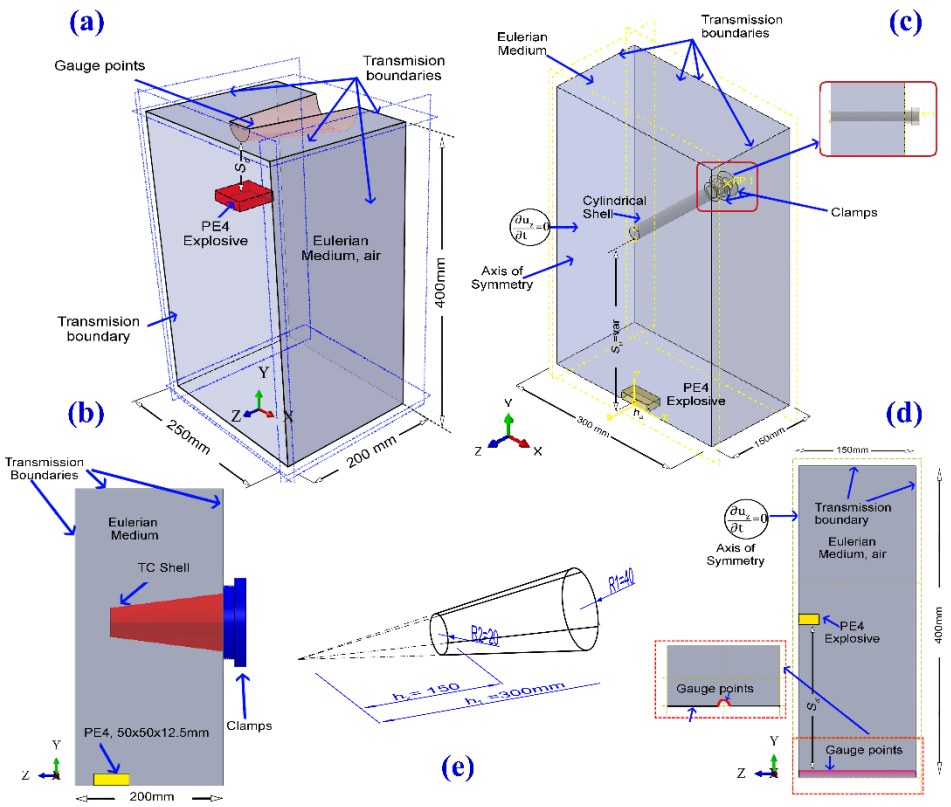

Figure 1. Schematics of the FSI model (a, b) CEL and UEL models of cylindrical shell, respectively, (c, d) UEL and CEL models of the TC shell, respectively, (e) Geometry of the TC

The Young modulus and Poisson's ratio of both shell types were 200GPa, and 0.3 respectively. While these shells were discretised using generic doubly curved reduced integration shell elements S4R and had the same thickness of 4mm, the characteristic elemental length of the cylindrical shells was 1.2mm while that of the TC shell rose from 1.2mm at the free end to 2.4mm at the fixed end. As the structural response transpires in a short period during the blast loading, an adiabatic thermodynamic process may be assumed, suggesting a typical value for the Taylor Quinney coefficient as 0.9. This coefficient evaluates the fraction of the plastic work that is converted to heat which is assumed in this case 90%. The remaining fraction of the energy extended and absorbed in the structure is used for structural reconfiguration.

Notably, the smaller size of the Lagrangian element compared with that of the Eulerian element not only satisfies the convergence of the displacement field and associated state variables in the shell but can also validate the credibility of the FSI model and correct coupling of the Lagrangian algorithms with Eulerian ones, i.e., ensuring that no material leakage occurs in the model. Material leakage refers to a phenomenon where the blast pressure passes through the Lagrangian elements without the rupture of the later elements.

4. RESULTS AND DISCUSSIONS

The transient deformations of the shells are illustrated in Figure 2. Upon experiencing the extensive pressure, a dimple forms in the shell, the profile of which is symmetric with respect to the normal axis connecting the charge centroid to the centre of the shell. For distal blasts ($d = S_d/2L_e > 1.75$), the profile of the shell varies significantly with the generalised polar coordinate θ for proximal blasts (Figure) but remains independent of θ for rather distal blasts. Hence, the theoretical analysis by Wierzbicki [47] remains valid for the latter type of loading, provided the shell's vibration remains dominantly plastic. In other words, the criterion of this condition is the quotient of the elastic energy absorbed to the plastic energy dissipated must be infinitesimal. As a result, the residual vibrations and spring-back of the structure are maintained small compared to maximum diametric deformation at the tip of the shell. The shell tip point exhibits maximum equivalent plastic strain ε_{eq} and a plastic hinge develops.

However, as illustrated in Figure 2, as the stand-off increases, higher fluctuations in the transient deformations are observed, and the available theoretical analysis conditions to predict the plastic collapse of cylindrical shells will be violated. This confines these analyses to a limited range of stand-offs and necessitates for the development of more generic analytical models.

Table 2. Summary of the results from CEL and UEL analyses

Shell type	S_d/L	**Impulse I_s(N.s)**			**Max P_0 (MPa)**	I_t $(\mu.s)$	**Diametric deformation W (mm)**
		Average	**Max**	**Min**			
Truncated Conical	0.75	22.97	25.37	21.21	721.33	14.55	29.30
	1.25	17.56	18.40	9.20	553.55	15.26	16.73
	1.75	9.95	14.21	7.11	281.07	17.58	8.05
	2.75	7.36	8.29	3.68	146.83	21.00	2.40
	3.75	4.59	5.11	3.68	29.30	31.01	1.10
Cylindrical	0.75	16.74	16.76	12.70	1004.31	9.35	Torn
	1.25	10.36	13.15	8.83	638.00	10.56	33.70
	1.75	8.81	8.60	3.49	299.39	14.76	21.32
	2.75	7.79	7.53	1.36	221.89	12.39	6.96
	3.75	7.72	5.60	4.69	150.40	10.54	3.55

The impulse and deformation values of the conical and cylindrical shells are summarised in Table 2 and compared in Figure . Notably, for the same stand-off distance and charge mass, the conical shells experienced smaller magnitudes of pressures but higher impulses due to the increased surface area. The preliminary observations of the FE results revealed that even though the maximum diametric deformation was registered with the flexible target mesh points closest to the explosive extreme fibre, the maximum pressure was registered not with the corresponding gauge point of the rigid target, but with the elements to the right and left of this gauge point. This is because the initial curvature of these form-active shells causes blast wave dispersions. As a result, the computed impulse based on Eq. (5) and (6) yields different values. In general, when the pressure distribution to either side of the shell was not uniform, the elements to the left side experienced higher pressure. The maximum and minimum impulses were then computed by consideration of the upper and lower bounds of outer face gauge pressures P_0 and utilising Eq. (6). It should, however, be noted that due to the variation of the shell radius and hence the element area A_{el} of TC shells, the accurate estimation of the impulse becomes cumbersome. Thus, the average impulse values in Table 2 are associated with the average elemental area of the blast projection points. An upper bound estimate of impulse may be computed by considering impulsive load and capturing the blast duration from pressure time history graphs. However, this method may lead to inaccurate results in the case of distal blasts, as the nature of the distal load will become dynamic, rather than remaining impulsive.

The variations and skewness of computed impulses are illustrated in Figure . The variation of impulse standard deviations is also erratic and varies from 2.09 and 2.33 for the most proximal blasts on TC and cylindrical shells, respectively, to the minimum of 0.72 and 1.55 for most distal blasts on these shells, respectively. The maximum standard deviations are calculated as 5.08 and 3.69 for S_d/D_e of 1.25 and 2.75 concerning the TC and cylindrical shells, respectively. It should be noted that, while the method developed herein for the computation of the average impulse is consistent with that of [17] for the square plates and in good agreement with their experimental results, experiments are required to accurately capture the impulse imparted to the shells for a range of stand-offs and particularly for the more distal blasts, when the FSI effects and boundary conditions contribute to the reduction of the impulse computed from the UEL methods.

A general trend of shell behaviour upon variation of stand-off is the reduction of permanent shell deformations, an increase of the blast duration (and the temporal component of impulse i_t, accordingly), significant reductions of the maximum gauge pressures and linear decrease of total imparted impulse on the shell, which is concurrent with the results of [48]–[51]. Due to the higher structural stiffness and mass, the TC shells experienced lower deformations than the cylindrical ones. The most proximal blast tore the cylindrical shell but the corresponding maximum deformation of the TC shell, in this case, was even lower than that of the cylindrical shell with a larger stand-off of 62.5mm. Furthermore, the gain of the deflections at the expense of impulse increase is more pronounced for the cylindrical shells. With the increase of stand-off distance to 187.5mm, the maximum gauge pressure of cylindrical shells reduces to 15% of its value for $S_d = 37.5mm$. The trend of pressure variation remains abrupt until the threshold stand-off ratio of ~1.75 is reached beyond which the nature of pressure variation (and other state variables) transitions to smooth.

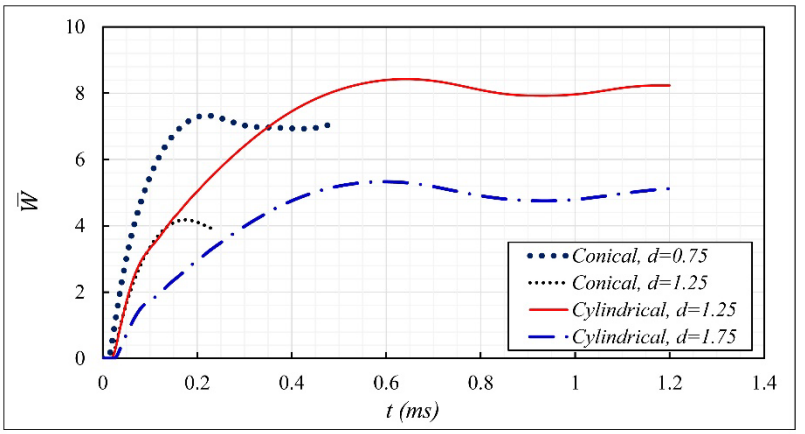

(a)

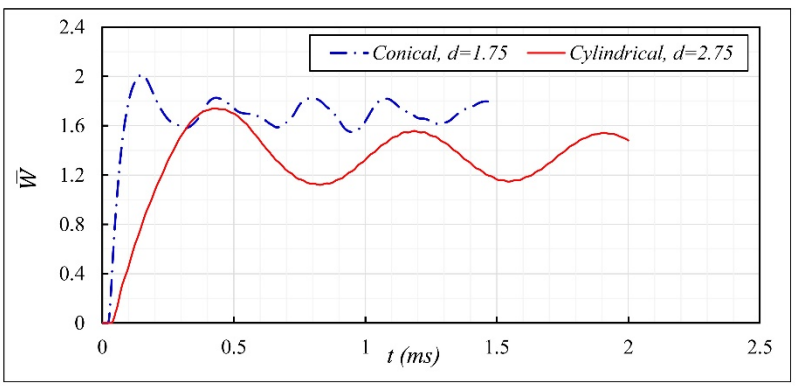

(b)

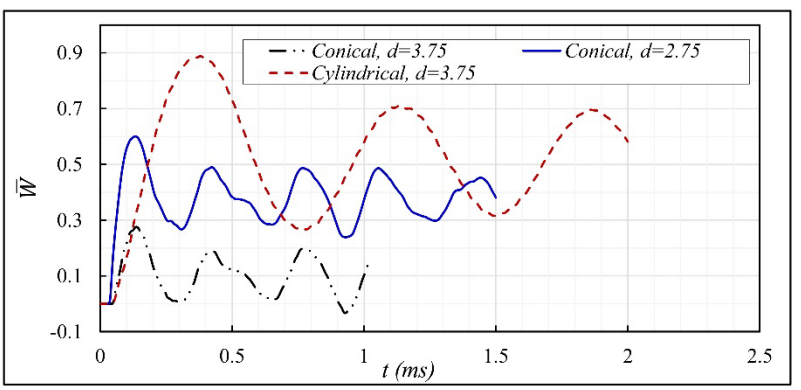

(c)

Figure 2. Transient deformation of the TC and cylindrical shells due to, (a) proximal, (b, c) distal blasts

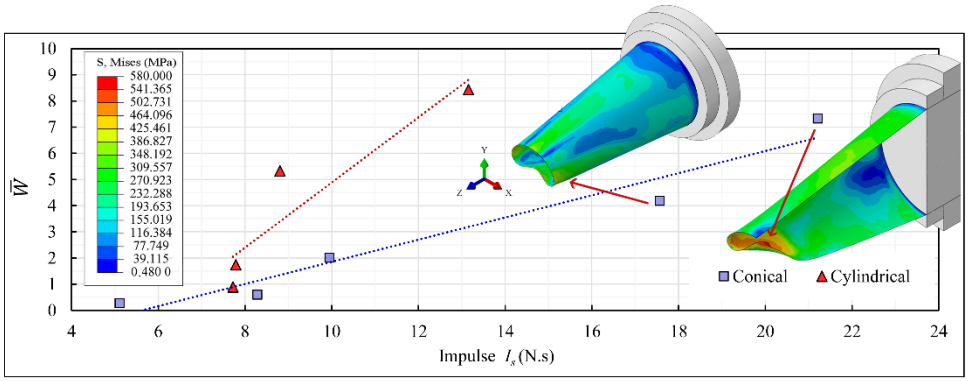

Figure 3. Variation of the shell impulse with maximum diametric deformation

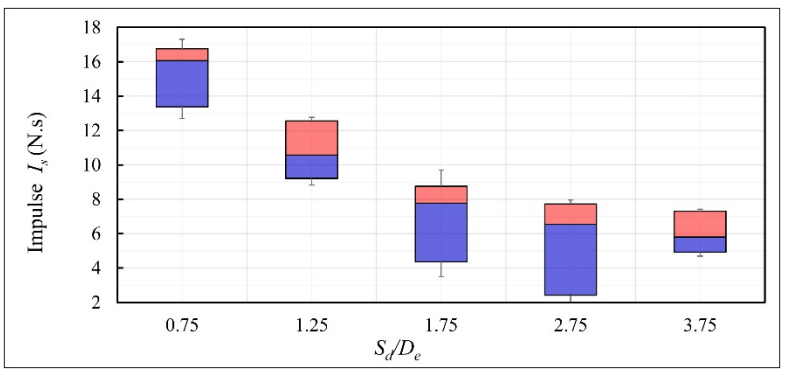

(a)

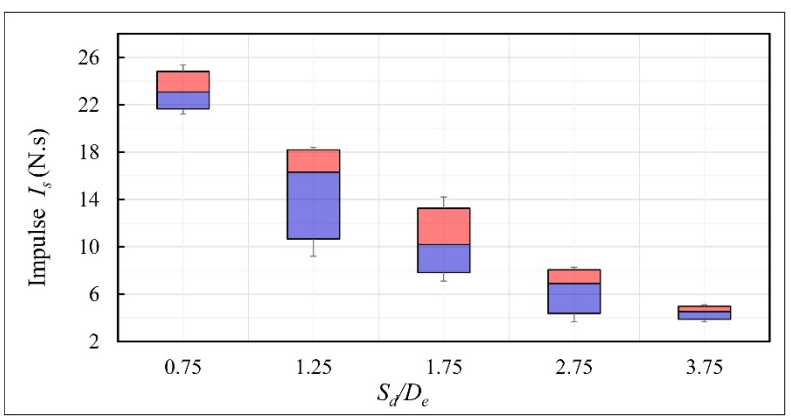

(b)

Figure 4. (a) Cylindrical shell box whiskers plot, (b) TC shell box-whiskers plot

The variation of the pulse shape exponent X with stand-off for a constant duration of $t_d = 30\mu s$, is plotted in Figure 5b which depicts a decrease in the value of this parameter with increasing dimensionless stand-off. This reduction in X is, nonetheless; offset by the increase in the pulse duration, causing a rather exponential increase in the pulse shape impulse (Figure 5c). The curve fitting expression of pulse shape impulse component reads:

$$i_t = \exp\left(-\frac{0.771 S_d}{D_e}\right) + 12.96, \tag{12}$$

An approximate fit to the function f_1 with good precision can be expressed as:

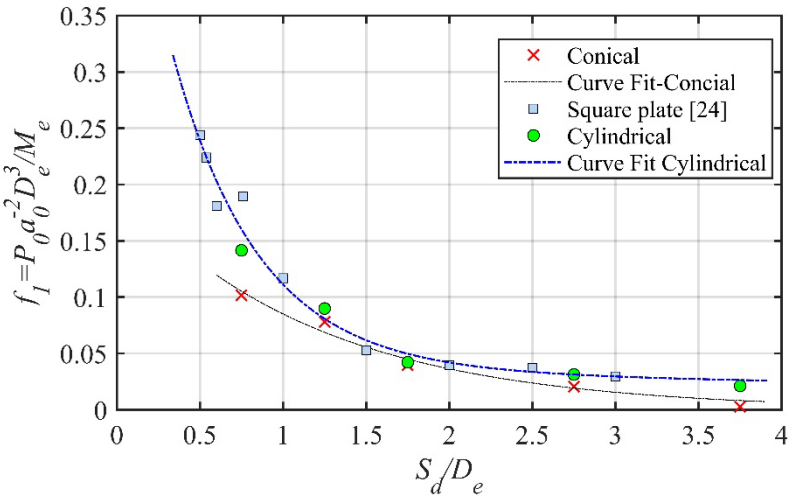

(a)

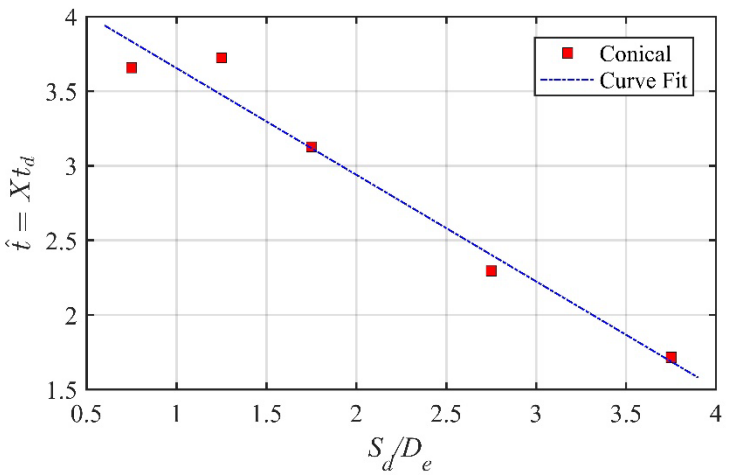

(b)

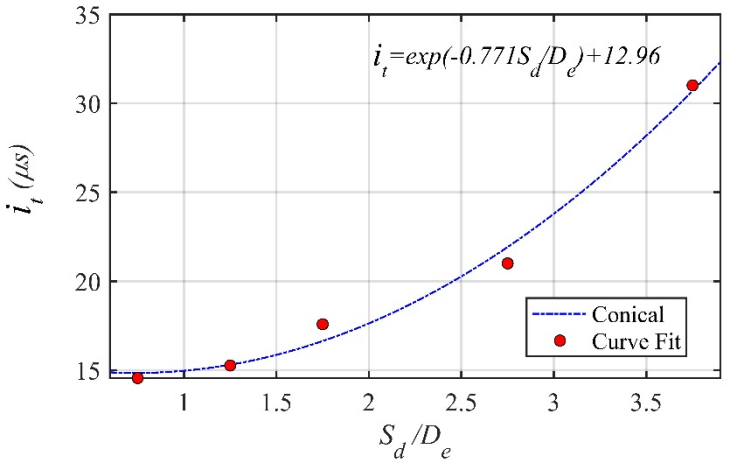

(c)

Figure 5 (a) Curve fitting of the f_1 function cylindrical and conical shells with function of Eq. ((14)) (b) variation of the pulse coefficient X with stand-off distance, (c) variation of the temporal ipulse component with stand-off distance

$$f_1 = a_1 exp\left(b_1 \frac{S_d}{D_e}\right), \tag{13}$$

where $a_1 = 0.199, b_1 = -0.850$ for the conical section.

The values of parameters above in f_1 for the cylindrical shells are close to those for the square plates given by [27] and the same function (i.e., $f_1 = 0.11(S_d/D_e)^{-1.153}$ may be used. A more accurate curve fitted expression, as shown in Figure 5a, which can unify the two results with an R^2 =96.5% coefficient of confidence is given as:

$$f_1 = a_2 exp\left(b_2 \frac{S_d}{D_e}\right) + c_2 exp\left(d_2 \frac{S_d}{D_e}\right), \tag{14}$$

with $a_2 = 0.54$, $b_2 = -1.94$, $c_2 = 0.0374$, and $d_2 = -0.0975$.

In agreement with the results of [26], [27], [35], the maximum diametric deformation of the shells at the tip of the contact interface increases rather exponentially with the reduction in the stand-off distance. The abrupt increase is more pronounced when the threshold limit of the stand-off reciprocal ($D_e/S_d \sim 2/3$) is surpassed. While it should be stressed that the exact threshold stand-off value depends on the topology and shape of the target structure, geometrical and material properties of the explosive, and the medium within which the blast wave advection occurs, the blast loads with dimensionless stand-off below the range 1.47 [35] can be labelled as localised for which the structural design must be treated with caution due to the added complexities of strain localisation, load distribution, and impulse concentration over a smaller contact zone. Because of these features, the localised blast loads would give rise to different modes of failure than the global ones.

The empirical expression for the dimensionless impulse which disregards the influence of stand-off (Figure 6a) for conical shells is given as:

$$\phi_c = 0.402\bar{W} - 2.53, \tag{15}$$

and for the cylindrical shells:

$$\phi_c = 2.66\bar{W} - 13.8, \tag{16}$$

The expression of ϕ_c for conical shells is closer to the empirical expression proposed by Nurick and Martin [28] for the plates ($\phi_c = 0.425\bar{W}$) than that of the cylindrical shells. When the influence of stand-off distance is retained in the analyses, the expressions for the dimensionless impulse for conical and cylindrical shells, respectively, read:

$$\phi_{sd} = 0.459\bar{W} - 0.622, \tag{17}$$

$$\phi_{sd} = 2.94\bar{W} - 5.32, \tag{18}$$

The significant difference between the FE results and the empirical models on various structural elements hitherto in the literature necessitates performing analytical studies. However, the few analytical models pioneered by Wierzbicki [52], [53] on locally blast loaded cylindrical shells oversimplify the case by greatly reducing the various parameters or phenomena influencing the shells' response, i.e., FSI, strain rate sensitivity, shear deformation variations, and stand-off distance.

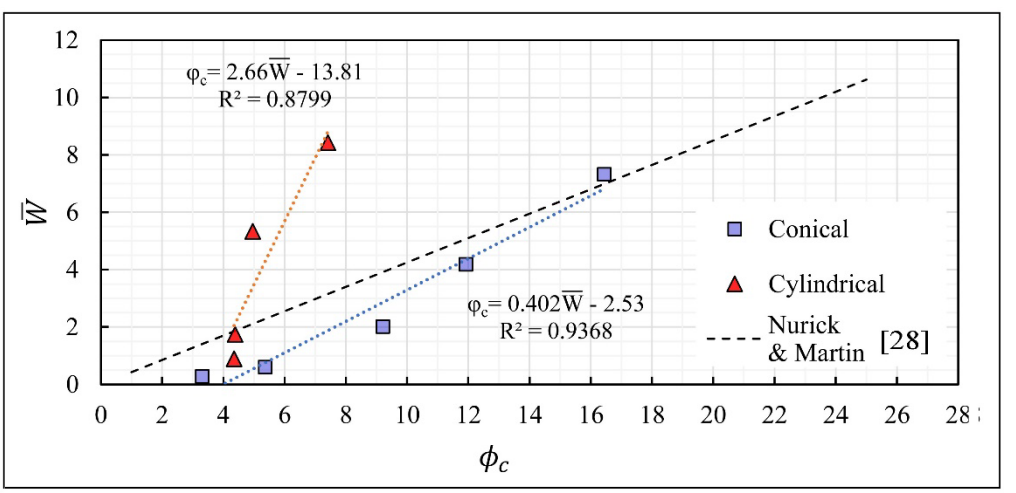

(a)

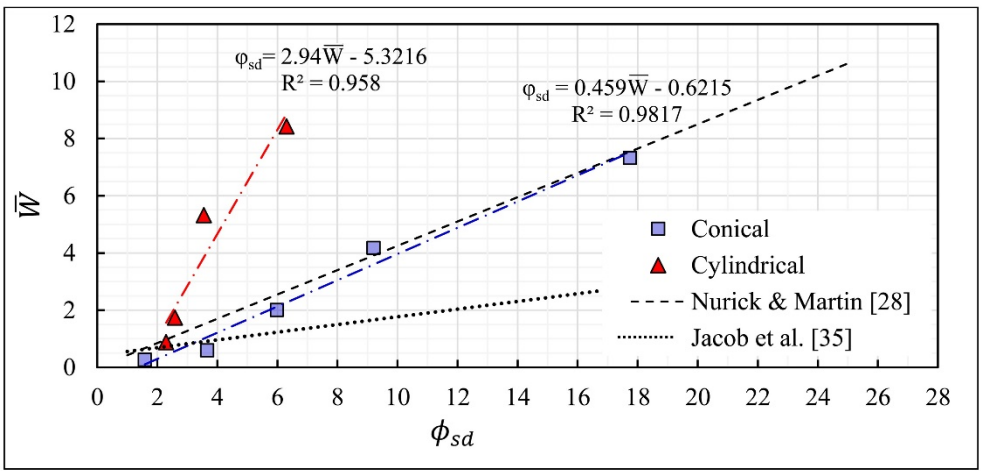

(b)

Figure 6. variation of the dimensionless impulse with diametric deformations of the shells, (a) by disregarding the influence of stand-off (b) by retaining the influence of stand-off.

5. CONCLUSIONS

This work dealt with the dynamic response of truncated conical and cylindrical shells subjected to a range of blast loads, from localised to global ones, induced by external PE4 explosives. The multiphysics of the blast pressure and target response was examined through coupled and uncoupled FSI analyses.

The blast load properties and the target response were expressed as sets of dimensionless functions which depended on the stand-off to (equivalent) charge diameter ratio d. To this end, the blast load was assumed to be representable as a multiplicative function of its temporal and spatial parts, in other words a truncated series cut off at its first term. While the temporal impulse component increased significantly with the increase of stand-off distance, the total pressure and exerted impulse reduced significantly up to the threshold $d = 1.75$, followed by a rather smooth variation. Such a value may be perceived as a transition stand-off which highlights the distinguishable difference in the response of the structural frameworks.

The parameters of the dimensionless functions were determined by using the Curve-Fitting tools on the FE results, and empirical linear relationships between the impulse and shell diametric deformation, and exponential one in the pressure magnitude with stand-off distance were observed. As expected, an increase in the shell diametric deformation with a decrease in stand-off was observed. Furthermore, the shells subjected to localised blasts exhibited a dimple profile with significant variation in the permanent deformation across the polar coordinate θ and little fluctuations in the landscape of deformation time histories. On the other hand, the shells subjected to distal blasts exhibited a rather flat profile with higher fluctuations in the transient deformation plots.

The results here supplement the previous results of the authors in [27] and serve as empirical models whereby the TC and cylindrical shells responses within a moderate range of blast load types can be predicted, from localised ($d = 0.75$) to global ($d > 1.75$).

REFERENCES

[1] S. C. K. Yuen et al., "Response of Cylindrical Shells to Lateral Blast Load," Int. J. Prot. Struct., vol. 4, no. 3, pp. 209–230, Sep. 2013.

[2] Q. M. Li and N. Jones, "Blast loading of a 'short' cylindrical shell with transverse shear effects," Int. J. Impact Eng., vol. 16, no. 2, pp. 331–353, 1995.

[3] J. M. Brett and G. Yiannakopolous, "A study of explosive effects in close proximity to a submerged cylinder," Int. J. Impact Eng., vol. 35, no. 4, pp. 206–225, 2008.

[4] J. M. Brett, G. Yiannakopoulos, and P. J. van der Schaaf, "Time-resolved measurement of the deformation of submerged cylinders subjected to loading from a nearby explosion," Int. J. Impact Eng., vol. 24, no. 9, pp. 875–890, 2000.

[5] D. Redekop and P. Azar, "Dynamic response of a cylindrical shell panel to explosive loading," J. Vib. Acoust. Trans. ASME, vol. 113, no. 3, pp. 273–278, 1991.

[6] J. Jiang and M. D. Olson, "New design-analysis techniques for blast loaded stiffened box and cylindrical shell structures," Int. J. Impact Eng., vol. 13, no. 2, pp. 189–202, 1993.

[7] S. K. Clubley, "Non-linear long duration blast loading of cylindrical shell structures," Eng. Struct., vol. 59, pp. 113–126, 2014.

[8] M. S. Hoo Fatt and H. Surabhi, "Blast resistance and energy absorption of foam-core cylindrical sandwich shells under external blast," Compos. Struct., vol. 94, no. 11, pp. 3174–3185, 2012.

[9] C. F. Hung, B. J. Lin, J. J. Hwang-Fuu, and P. Y. Hsu, "Dynamic response of cylindrical shell structures subjected to underwater explosion," Ocean Eng., vol. 36, no. 8, pp. 564–577, 2009.

[10] K. M. Liew, C. W. Lim, and L. S. Ong, "Flexural vibration of doubly-tapered cylindrical shallow shells," Int. J. Mech. Sci., vol. 36, no. 6, pp. 547–565, 1994.

[11] K. R. Sivadas and N. Ganesan, "Free vibration of circular cylindrical shells with axially varying thickness," J. Sound Vib., vol. 147, no. 1, pp. 73–85, 1991.

[12] A. Ibrahim, Y. Ryu, and M. Saidpour, "Stress Analysis of Thin-Walled Pressure Vessels," Mod. Mech. Eng., vol. 5, no. February, pp. 1–9, 2015.

[13] G. P. Kouretzis, G. D. Bouckovalas, and C. J. Gantes, "Analytical calculation of blast-induced strains to buried pipelines," Int. J. Impact Eng., vol. 34, no. 10, pp. 1683–1704, 2007.

[14] P. Neuwald, H. Reichenbach, A. L. Kuhl, and F. Institut, "Combustion of Shock-Dispersed Flake-Aluminum in a Long Tunnel Section," in 20th Int Colloq Dynamics of Explosions and Reactive Systems, Jan. 2005, pp. 1–4.

[15] S. Li, G. Lu, Z. Wang, L. Zhao, and G. Wu, "Finite element simulation of metallic cylindrical sandwich shells with graded aluminum tubular cores subjected to internal blast loading," Int. J. Mech. Sci., vol. 96–97, no. March, pp. 1–12, 2015.

[16] T. Duffey and D. Mitchell, "Containment of explosions in cylindrical shells," Int. J. Mech. Sci., vol. 15, no. 3, pp. 237–249, 1973.

[17] N. Mehreganian, L. A. Louca, G. S. Langdon, R. J. Curry, and N. Abdul-Karim, "The response of mild steel and armour steel plates to localised air-blast loading-comparison of numerical modelling techniques," Int. J. Impact Eng., vol. 115, no. January, pp. 81–93, 2018.

[18] G. S. Langdon, W. C. Lee, and L. A. Louca, "The influence of material type on the response of plates to air-blast loading," Int. J. Impact Eng., vol. 78, pp. 150–160, 2015.

[19] Y. W. Kwon and P. K. Fox, "Underwater shock response of a cylinder subjected to a side-on explosion," Comput. Struct., vol. 48, no. 4, pp. 637–646, 1993.

[20] H. Saunders, E. J. Wisniewski, and P. R. Paslay, "Vibrations of Conical Shells," J. Acoust. Soc. Am., vol. 32, no. 6, pp. 765–772, Jun. 1960.

[21] C. C. Yang, "On vibrations of orthotropic conical shells," J. Sound Vib., vol. 34, no. 4, pp. 552–555, 1974.

[22] Q. M. Li and N. Jones, "On dimensionless numbers for dynamic plastic response of structural members," Arch. Appl. Mech., vol. 70, no. 4, pp. 245–254, 2000.

[23] N. Jones, Structural Impact. Cambridge: Cambridge University Press, 1989.

[24] Y.-P. Zhao, "Suggestion of a new dimensionless number for dynamic plastic response of beams and plates," Arch. Appl. Mech., vol. 68, no. 7–8, pp. 524–538, 1998.

[25] C. K. Youngdahl, "Correlation parameters for eliminating the effects of pulse shape on dynamic plate deformation," Trans. ASME J. Appl. Mech., vol. 37, no. 2, pp. 744–752, 1970.

[26] K. Micallef et al., "On dimensionless loading parameters for close-in blasts," Int. J. Multiphys., vol. 9, no. 2, p. 193, 2015.

[27] N. Mehreganian, A. S. S. Fallah, G. K. K. Boiger, and L. A. A. Louca, "Response of Armour Steel Square Plates To Localised Air Blast Load- a Dimensional Analysis," Int. J. Multiphys., vol. 11, no. 4, pp. 1–20, 2017.

[28] S. C. K. Yuen and G. N. Nurick, "Experimental and numerical studies on the response of quadrangular stiffened plates. Part I: Subjected to uniform blast load," Int. J. Impact Eng., vol. 31, no. 1, pp. 55–83, 2005.

[29] R. G. Teeling-Smith and G. N. Nurick, "The deformation and tearing of thin circular plates subjected to impulsive loads," Int. J. Impact Eng., vol. 11, no. 1, pp. 77–91, 1991.

[30] G. N. Nurick and J. B. Martin, "Deformation of thin plates subjected to impulsive loading - A review - Part II - Experimental results," Int. J. Impact Eng., vol. 8, no. 2, pp. 171–186, 1989.

[31] G. N. Nurick and J. B. Martin, "Deformation of thin plates subjected to impulsive loading-A review. Part I: Theoretical considerations," Int. J. Impact Eng., vol. 8, no. 2, pp. 159–170, 1989.

[32] S. Chung Kim Yuen, G. N. Nurick, G. S. Langdon, and Y. Iyer, "Deformation of thin plates subjected to impulsive load: Part III – an update 25 years on," Int. J. Impact Eng., vol. 107, pp. 1339–1351, 2017.

[33] G. N. Nurick, S. Mahoi, and G. S. Langdon, "The response of plates subjected to loading arising from the detonation of different shapes of plastic explosive," Int. J. Impact Eng., vol. 89, no. November, pp. 102–113, 2016.

[34] S. Chung Kim Yuen, G. S. Langdon, G. N. Nurick, E. G. Pickering, and V. H. Balden, "Response of V-shape plates to localised blast load: Experiments and numerical simulation," Int. J. Impact Eng., vol. 46, pp. 97–109, 2012.

[35] N. Jacob, G. N. Nurick, and G. S. Langdon, "The effect of stand-off distance on the failure of fully clamped circular mild steel plates subjected to blast loads," Eng. Struct., vol. 29, no. 10, pp. 2723–2736, 2007.

[36] B. M. Dobratz, "Properties of chemical explosives and explosive simulants," Lawrence Livermore Natl. Lab., vol. 1, pp. 1–334, 1972.

[37] K. Micallef, A. Soleiman Fallah, D. J. Pope, M. Moatamedi, and L. A. Louca, "On dimensionless loading parameters for close-in blasts," Int. Jounral Multiphysics, vol. 9, no. 2, pp. 171–194, 2015.

[38] N. Jones, "Dynamic inelastic response of strain rate sensitive ductile plates due to large impact, dynamic pressure and explosive loadings," Int. J. Impact Eng., vol. 74, pp. 3–15, 2014.

[39] D. Bonorchis and G. N. Nurick, "The influence of boundary conditions on the loading of rectangular plates subjected to localised blast loading - Importance in numerical simulations," Int. J. Impact Eng., vol. 36, no. 1, pp. 40–52, 2009.

[40] G. S. Langdon, A. Ozinsky, and S. C. K. Yuen, "The response of partially confined right circular stainless steel cylinders to internal air-blast loading," Int. J. Impact Eng., vol. 73, no. May, pp. 1–14, 2014.

[41] N. Mehreganian, M. Toolabi, Y. A. Zhuk, F. Etminan Moghadam, L. A. Louca, and A. S. Fallah, "Dynamics of pulse-loaded circular Föppl-von Kármán thin plates-Analytical and numerical studies," J. Sound Vib., vol. 513, p. 116413, 2021.

[42] V. Aune, G. Valsamos, F. Casadei, M. Larcher, M. Langseth, and T. Børvik, "Numerical study on the structural response of blast-loaded thin aluminium and steel plates," Int. J. Impact Eng., vol. 99, pp. 131–144, 2017.

[43] G. I. Taylor, "The pressure and Impulse of Submarine Explosion Waves on Plates," in The scientific papers of Sir Geoffrey Ingram Taylor: Vol 3 Aerodynamics and the Mechanics of Projectiles and Explosions, vol. III, no. 4, G. K. . Batchelor, C. F. . Sharman, J. W. . Maccoll, R. M. . Davies, H. ; Jones, and P. G. . Saffman, Eds. Cambridge, UK: Cambridge University Press, 2011, p. 590.

[44] N. Kambouchev, R. Radovitzky, and L. Noels, "Fluid–Structure Interaction Effects in the Dynamic Response of Free-Standing Plates to Uniform Shock Loading," J. Appl. Mech., vol. 74, no. 5, p. 1042, 2007.

[45] N. Mehreganian, A. S Fallah, and L. A. Louca, "Inelastic dynamic response of square membranes subjected to localised blast loading," Int. J. Mech. Sci., vol. 148, no. November, pp. 578–595, 2018.

[46] N. . Mehreganian, G. K. Boiger, M. . Moatamedi, and A. . S Fallah, "Dynamic analysis of cylindrical shells subject to multiple blasts using FSI," Int. J. Multiphys., vol. 15, no. 4, pp. 453–476, 2021.

[47] M. S. Hoo Fatt and T. Wierzbicki, "Damage of plastic cylinders under localized pressure loading," Int. J. Mech. Sci., vol. 33, no. 12, pp. 999–1016, 1991.

[48] G. S. Langdon, S. C. K. Yuen, and G. N. Nurick, "Experimental and numerical studies on the response of quadrangular stiffened plates. Part II: Localised blast loading," Int. J. Impact Eng., vol. 31, no. 1, pp. 85–111, 2005.

[49] S. Chung Kim Yuen and G. N. Nurick, “The significance of the thickness of a plate when subjected to localised blast loads,” Blast Impact Load. Struct., pp. 471–499, 2000.

[50] G. N. Nurick and G. C. Shave, “The deformation and tearing of thin square plates subjected to impulsive loads - An experimental study,” Int. J. Impact Eng., vol. 18, no. 1, pp. 99–116, 1996.

[51] G. N. Nurick and A. M. Radford, “Deformation and tearing of clamped circular plates subjected to localised central blast loads,” Recent Dev. Comput. Appl. Mech. a Vol. honour John B. Martin, pp. 276–301, 1997.

[52] T. Wierzbicki and M. S. Hoo Fatt, “Damage assessment of cylinders due to impact and explosive loading,” Int. J. Impact Eng., vol. 13, no. 2, pp. 215–241, 1993.

[53] T. Wierzbicki and G. N. Nurick, “Large deformation of thin plates under localised impulsive loading,” Int. J. Impact Eng., vol. 18, no. 96, pp. 899–918, 1996.